

## HOROLOGIUM II: A SECOND ULTRA-FAINT MILKY WAY SATELLITE IN THE HOROLOGIUM CONSTELLATION

DONGWON KIM AND HELMUT JERJEN

Research School of Astronomy and Astrophysics, The Australian National University, Mt Stromlo Observatory, via Cotter Rd, Weston, ACT 2611, Australia

*Draft version July 8, 2015*

### ABSTRACT

We report the discovery of a new ultra-faint Milky Way satellite candidate, Horologium II, detected in the Dark Energy Survey Y1A1 public data. Horologium II features a half light radius of  $r_h = 47 \pm 10$  pc and a total luminosity of  $M_V = -2.6_{-0.3}^{+0.2}$  that place it in the realm of ultra-faint dwarf galaxies on the size-luminosity plane. The stellar population of the new satellite is consistent with an old ( $\sim 13.5$  Gyr) and metal-poor ( $[\text{Fe}/\text{H}] \sim -2.1$ ) isochrone at a distance modulus of  $(m - M) = 19.46 \pm 0.20$ , or a heliocentric distance of  $78 \pm 8$  kpc, in the color-magnitude diagram. Horologium II has a distance similar to the Sculptor dwarf spheroidal galaxy ( $\sim 82$  kpc) and the recently reported ultra-faint satellites Eridanus III ( $87 \pm 8$  kpc) and Horologium I ( $79 \pm 8$  kpc). All four satellites are well aligned on the sky, which suggests a possible common origin. As Sculptor is moving on a retrograde orbit within the Vast Polar Structure when compared to the other classical MW satellite galaxies including the Magellanic Clouds, this hypothesis can be tested once proper motion measurements become available.

*Subject headings:* Local Group - Galaxy: halo - galaxies: dwarf - galaxies: individual (Horologium II) - galaxies: stellar content

### 1. INTRODUCTION

Over the last decades wide-field imaging surveys have systematically revealed new satellite companions to the Milky Way (MW). Especially, the Sloan Digital Sky Survey (SDSS; York et al. 2000) was instrumental in establishing a new class of stellar systems, the ultra-faint dwarf (UFD) galaxies (e.g. Willman et al. 2005; Zucker et al. 2006; Belokurov et al. 2006; Irwin et al. 2007; Walsh et al. 2007; Grillmair 2009), thereby more than doubling the number of known MW satellite galaxies over half the northern hemisphere. Deep imaging follow-ups and spectroscopic studies suggest that the UFDs hold typically old (e.g. Muñoz et al. 2010; Sand et al. 2012; Brown et al. 2014) and metal poor (e.g. Kirby et al. 2008; Frebel et al. 2010; Norris et al. 2010) stellar populations. The high mass-to-light ratios of the UFDs ( $M/L_V > 100$ ) inferred from internal kinematics (e.g. Martin et al. 2007; Simon & Geha 2007; Simon et al. 2011) is one of properties that differentiate them from star clusters (Willman & Strader 2012). The efforts to find new MW satellites over a larger area of sky continued with the VST ATLAS (Shanks et al. 2015) and Pan-STARRS 3 $\pi$  (K. Chambers et al., in preparation) surveys, both of which have delivered a couple of discoveries to date (Belokurov et al. 2014; Laevens et al. 2014, 2015). Most recently, systematic searches based on the first data release (Y1A1) of the Dark Energy Survey (DES; The Dark Energy Survey Collaboration 2005), have continued the success of its predecessor the SDSS, unveiling nine new objects over  $\sim 1800$  square degrees in the southern sky (Koposov et al. 2015a; Bechtol et al. 2015)<sup>1</sup>, some of which have been already con-

firmed as UFDs by spectroscopic investigations (Simon et al. 2015; Walker et al. 2015; Koposov et al. 2015b). Other independent surveys, such as the Stromlo Missing Satellite Survey (Jerjen 2010) and the Survey of the Magellanic Stellar History (SMASH; D. Nidever et al., in preparation), also took advantage of the power of the Dark Energy Camera (DECam) to boost the census of MW companions in the southern sky (Kim et al. 2015a; Martin et al. 2015).

The use of different detection algorithms also contributed significantly to the increase in the number of known MW satellites (Koposov et al. 2008; Walsh et al. 2009). Due to their extremely low surface brightness (Martin et al. 2008), UFDs would be difficult to characterised without the help of such specialised data mining techniques. Further improvements to the detection sensitivity even led to new discoveries of stellar systems hiding in the pre-existing SDSS data (e.g. Kim & Jerjen 2015; Kim et al. 2015b).

Here we announce the discovery of a new ultra-faint MW satellite galaxy candidate found in the DES Y1A1 data. We note that this object Horologium II (Hor II) does not correspond to any object in the previous studies by Koposov et al. (2015a) and Bechtol et al. (2015) or in catalogs including the NASA/IPAC Extragalactic Database and SIMBAD.

### 2. DATA REDUCTION AND DISCOVERY

DES is a deep photometric survey using the wide-field ( $\sim 3$  square degree) Dark Energy Camera (DECam) imager that consists of 62  $2\text{k} \times 4\text{k}$  CCD chips installed at the 4-m Blanco Telescope located at Cerro Tololo Inter-American Observatory (CTIO). DES started operation in August 2013 and will cover  $\sim 5000$  square degrees of the Southern Sky in the vicinity of the Magellanic Clouds in five photometric bands (*grizY*) over

dongwon.kim@anu.edu.au

<sup>1</sup> We note that the satellite reported as Indus I by Koposov et al. (2015a) and as DES J2108.8-5109 by Bechtol et al. (2015) is identical to Kim 2 that was discovered earlier by Kim et al. (2015a).

five years. The data used in this paper is its first year public data set, DESDM Y1A1, collected between August 2013 and February 2014 over approximately 1800 square degrees and released to the public by the NOAO Science archive after a one year proprietary period. This data set includes individual images and corresponding weight-maps processed by the DES data management (DESDM) pipeline. Each image is a 90s single exposure. The instCal images we used for our analysis are bias, dark and flat-field corrected and contain the world coordinate system provided by the DESDM image processing pipeline (see Desai et al. 2012; Mohr et al. 2012, for more details).

We downloaded all the Y1A1 instCal images and corresponding weight-maps for the  $g$  and  $r$  bands from the NOAO Science archive using its SQL interface. Cross-matching the central coordinates of the images within  $1'.0$  radius yielded 1980 image pairs between the two photometric bands. To produce photometric catalogs, we performed PSF photometry over the images using SExtractor/PSFEx (Bertin & Arnouts 1996; Bertin 2011) on a local 16 nodes/128 core computer cluster. We carried out star/galaxy separation based on the threshold  $|\text{SPREAD\_MODEL}| < 0.003 + \text{SPREADERR\_MODEL}$  as described in Koposov et al. (2015a). The catalogs, which contained the instrumental magnitudes of the star-like objects, were crossmatched between  $g$  and  $r$  bands by employing STILTS (Taylor 2005) with a  $1''$  tolerance. We then calibrated the instrumental magnitudes of the star-like point sources with respect to the APASS DR 8 stars by means of 500 bootstrap samples with 3-sigma clipping. On average, we found  $\sim 370$  crossmatches between the instrumental and APASS catalogs on each frame, which yielded photometric zero points with uncertainties  $\sim 0.003$  magnitudes in both  $g$  and  $r$  bands. The calibrated magnitudes were finally corrected for Galactic extinction using the reddening map by Schlegel et al. (1998) and the correction coefficients from Schlafly & Finkbeiner (2011).

We then applied our overdensity detection algorithm to the star catalogs to search for MW satellites. Briefly, this algorithm, following the approach by Walsh et al. (2009), involves a photometric filtering process in which an isochrone mask is applied to select a single age/metallicity stellar population at a fixed distance modulus. The density map generated from the selected stars is then convolved with a Gaussian kernel. The significance of local stellar overdensities is measured by comparing their signal-to-noise ratios to the smoothed density map. These steps are repeated shifting the isochrone mask over a range of distance moduli. The detection process is described in more details in Kim & Jerjen (2015). As part of this photometric analysis of the entire 1800 sqr deg of  $gr$  images of the Y1A1 data set, we successfully recovered all the UFD candidates reported by Koposov et al. (2015a) and Bechtol et al. (2015); e.g. Phoenix II ( $17\sigma$ ), Pictoris I ( $13\sigma$ ), Tucana II ( $11\sigma$ ), Eridanus III ( $10\sigma$ ), and Grus I ( $9\sigma$ ). We also found one additional MW satellite candidate in the constellation of Horologium. This new object, Horologium II, was initially detected at the  $7\text{--}8\sigma$  significance levels in two separate, but overlapping DECam images. To fill the CCD chip gaps, we combined the photometric catalogs of the two frames and removed duplicates with  $1''$  tolerance.

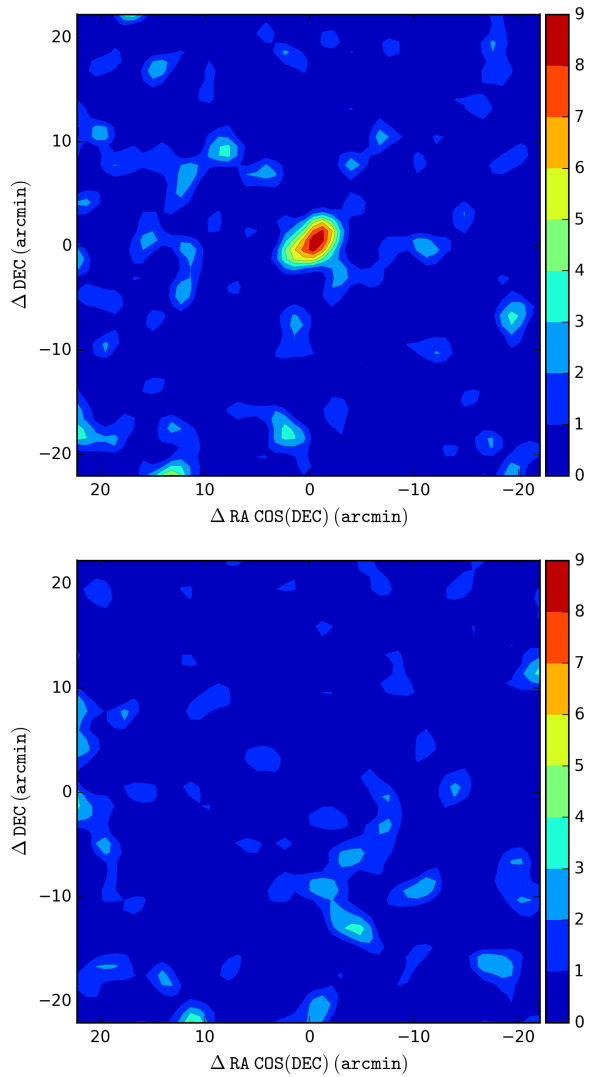


FIG. 1.— Upper panel: Smoothed density contour map of candidate stars, selected by the photometric filter with a PARSEC isochrone of 13.5 Gyr and  $[\text{Fe}/\text{H}] = -2.1$  (Bressan et al. 2012) shifted to the distance modulus  $(m - M) = 21.56$  magnitudes, centred on Hor II in the  $42 \times 42$  square arcmin window. The contours represent the stellar density in units of the standard deviation above the background level. Lower panel: Same as the upper panel but for non-stellar objects, showing no overdensity consistent with Hor II in the upper panel.

Hor II was then recovered with a significance of  $10\sigma$ .

The upper panel of Figure 1 presents the density contour map of Hor II, made from stars passing the isochrone filter. Hor II appears elongated but well defined by high level density contours ( $> 3\sigma$ ). The lower panel shows the corresponding contour map of non-stellar objects in the same field of view.

### 3. CANDIDATE PROPERTIES

The left panel of Figure 2 shows the distribution of all stellar objects in our photometric catalogs within a  $25' \times 25'$  window centred on Hor II. The small red rectangles indicate the six locations of residual CCD chip gaps where the two DES images provided no data. In the middle panel, we present the color-magnitude diagram (CMD) for the stars in the inner circle shown in the left panel, equal to the dashed circle in the upper panel of

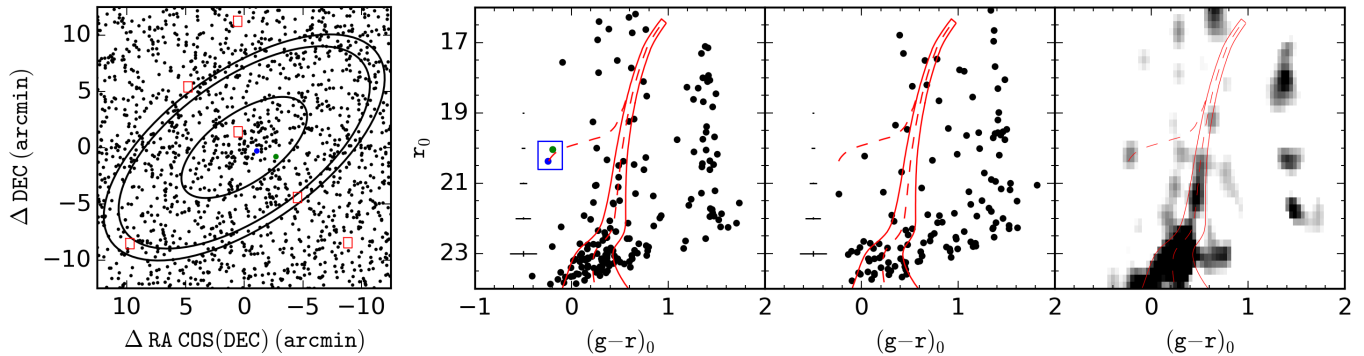


FIG. 2.— DECcam view of Hor II. Left panel: distribution of all stars in a  $25' \times 25'$  field centred on Hor II. The blue and green dots mark the two BHB candidates falling into the blue box in the next panel. The ellipses mark elliptical radii of  $6'.3$  ( $\sim 3r_h$ ),  $12'.6$  ( $\sim 6r_h$ ) and  $14'.1$  respectively. The red rectangles mark the locations of residual CCD chip gap where none of DES Y1A1 images covers. Middle left panel: CMD of stars lying in the inner circle. Overplotted is the best-fitting PARSEC (red dashed lines) isochrone of age 13.5 Gyr and  $[\text{Fe}/\text{H}]=-2.1$  shifted to the distance modulus of  $(m - M) = 19.46$ . Within the isochrone mask (red solid lines) based on photometric uncertainties, there are candidate stars consistently aligned with the isochrone from the RGB to the main sequence turn-off. The two BHB candidates are colored and correspond to those in the left panel. Middle right panel: control CMD of stars falling in the annulus between the two outer circles but covering the same on-sky area as in the middle panel. Right panel: differential Hess diagram, the inner CMD minus the control CMD, which exhibits a clear excess of stars in the RGB and the main sequence turn-off regions.

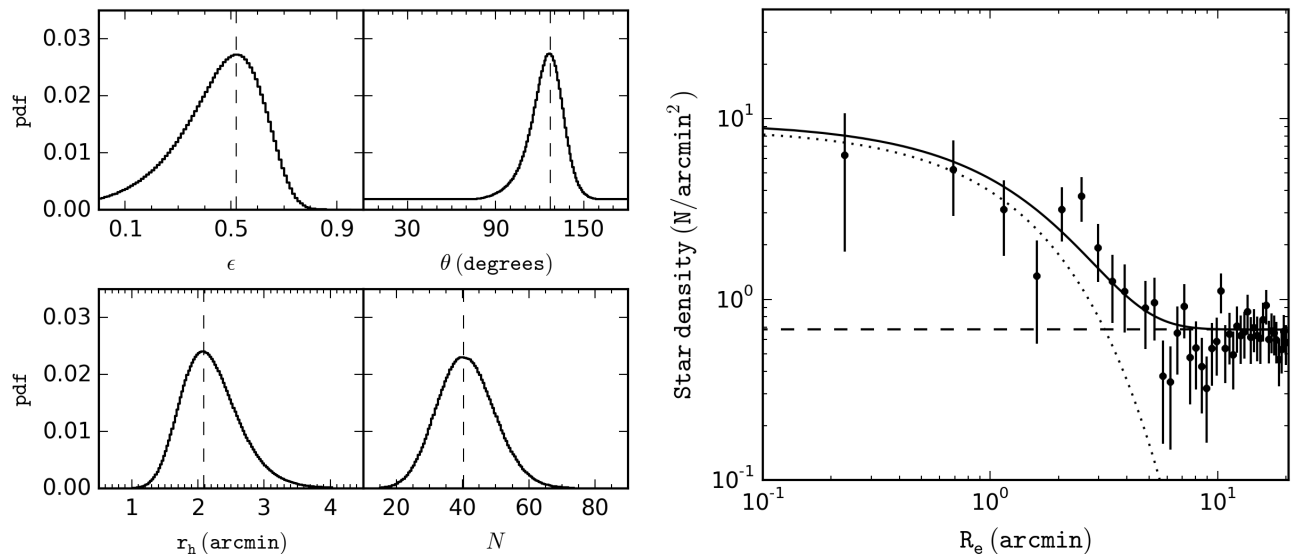


FIG. 3.— Left panels: marginalized probability distribution functions for the the ellipticity ( $\epsilon$ ), the position angle ( $\theta$ ), they half-light radius ( $r_h$ ) and the number of stars in the system for our photometric selection ( $N$ ). The dashed lines mark the modes of the distributions. Right panel: radial density profile of Hor II, constructed on the mode values of each parameter as a function of elliptical radius  $R_e$ . The error of each data point is based on Poisson statistics. The dotted line marks the best-fit exponential model, the dashed line the foreground level and the solid line the combined fit.

TABLE 1  
PROPERTIES OF HOROLOGIUM II

Parameter	Value	Unit
$\alpha_{J2000}$	$3\ 16\ 32.1 \pm 5.0$	h m s
$\delta_{J2000}$	$-50\ 01\ 05 \pm 5$	° ' "
$l$	$262.472$	deg
$b$	$-54.137$	deg
$(m - M)$	$19.46 \pm 0.20$	mag
$d_{\odot}$	$78 \pm 8$	kpc
$r_h$	$2.09^{+0.44}_{-0.41}$	'
	$47 \pm 10^a$	pc
$\epsilon$	$0.52^{+0.13}_{-0.17}$	
$\theta$	$127 \pm 11$	deg
$M_V$	$-2.6^{+0.2a}_{-0.3}$	mag

<sup>a</sup> Adopting a distance of 78 kpc

Figure 1. Overplotted is the PARSEC isochrone (Bresnan et al. 2012) of 13.5 Gyr and  $[\text{Fe}/\text{H}]=-2.1$  shifted to the distance modulus of  $(m - M) = 19.46 \pm 0.20$  or a heliocentric distance of  $78 \pm 8$  kpc. Compared to the control CMD established in the same manner as in Belokurov et al. (2006) shown in the right panel, the stars in the vicinity of Hor II consistently trace the old and metal-poor stellar population from the red-giant branch (RGB) down to the main-sequence turn off. Hor II also hosts two potential blue horizontal branch (BHB) stars.

We derived the structural parameters of Hor II using a Maximum Likelihood (ML) algorithm similar to the one described in Martin et al. (2008). The resulting marginalized pdfs for the structural parameters are presented in the left panels of Figure 3. The right panel shows the radial density profile with the best-fit expo-

ponential profile based on the best parameters; an ellipticity of  $\epsilon = 0.52$ , a position angle of  $\theta = 127^\circ$  and a half-light radius of  $r_h = 2'.09$ . Adopting the heliocentric distance of 78 kpc, the ML-estimated physical size of Hor II is  $r_h = 47 \pm 10$  pc.

The total luminosity of Hor II is estimated as follows. Briefly, we use the total number of member stars  $N$  above the photometric threshold ( $r_0 \sim 23.5$  mag) and its associated uncertainty derived from the ML algorithm run. We then integrate a normalised theoretical luminosity function as a probability density function of magnitude, by the same magnitude limit and use the ratio of the number  $N$  to the probability density to scale the luminosity function up to the observed level. Integrating the scaled luminosity function inclusive of missing flux below the threshold gives the absolute luminosity of Hor II. Using the PARSEC isochrone of 13.5 Gyr and  $[\text{Fe}/\text{H}] = -2.1$  based on the initial mass function by Kroupa (2001), we obtain  $M_r \sim -2.74$  or  $M_V \sim -2.57$  by the luminosity weighted mean color  $V - r = 0.17$  of the isochrone. We adopt a total luminosity of  $M_V = -2.6_{-0.3}^{+0.2}$  as our final estimate where its uncertainty is derived from the star counts  $N$ . All the resulting parameters are summarised in Table 1. We note that a heliocentric distance of 78 kpc was adopted in the calculations of the physical size and total luminosity, to which the distance uncertainty was not propagated.

#### 4. DISCUSSION AND CONCLUSION

We analysed the first instalment (Y1A1) of the Dark Energy Survey *gr* imaging data to search for MW satellites, where we recovered all the previously reported systems and also found a new satellite candidate in the constellation of Horologium. The new MW satellite candidate Hor II appears faint ( $M_V = -2.6_{-0.3}^{+0.2}$ ), elongated ( $\epsilon = 0.52_{-0.17}^{+0.13}$ ) and rather extended ( $r_h = 47 \pm 10$  pc). On the size luminosity plane, Hor II is placed in the realm of UFDs close to Boötes II. It also features a typically old ( $\sim 13.5$  Gyr) and metal-poor ( $[\text{Fe}/\text{H}] \sim -2.1$ ) stellar population. The best isochrone fit yields a heliocentric distance of  $78 \pm 8$  kpc, which is the same as that of a recently discovered neighbour in the DES Y1A1 coverage, Hor I. Compared to the new satellite candidate, Hor I is about twice as luminous ( $M_V = -3.4 \pm 0.3$ ), smaller ( $r_h = 30_{-3.3}^{+4.4}$  pc) and more circular ( $\epsilon < 0.28$ ), consequently being placed in the somewhat ambiguous region on the size-luminosity plane where UFDs and extended globular clusters overlap (Koposov et al. 2015a). A recent spectroscopic study by Koposov et al. (2015b) has revealed that the dynamical mass-to-light ratio of Hor I reaches  $M/L_V = 570_{-112}^{+1154}$  and confirmed that that system is indeed an UFD, possibly (once) associated with the LMC. The pair of UFDs, Hor I and II, are only  $\sim 7$  degrees away from each other on the sky, have identical distances and are well aligned with the Vast Polar Structure (Pawlowski et al. 2015). Such UFD pairs have been reported for quite some time e.g. Boötes I - II (Walsh et al. 2007), Leo IV - V (Belokurov et al. 2008) and Pisces II - Pegasus III (Kim et al. 2015b). The tentative link between Hor I and II can be extended further

to the Sculptor dwarf spheroidal ( $d_\odot \sim 82$  kpc, Weisz et al. 2014) and the UFD Eridanus III ( $d_\odot = 87 \pm 8$  kpc). As Sculptor is moving on a retrograde orbit within the Vast Polar Structure when compared to the other classical MW satellite galaxies in the vicinity, including the Magellanic clouds, the hypothesis of a common origin can be tested once proper motion measurements become available. Nevertheless, this alignment is already suggestive of a “layer” of outer halo UFDs parallel to the Magellanic Clouds, possibly associated to the most luminous Sculptor dwarf. Indeed, there is one more object nearby, namely Phe II, that also shares the same distance.

We thank the anonymous referee for the helpful comments and suggestions, which contributed to improving the quality of the publication. We acknowledge the support of the Australian Research Council through Discovery project DP150100862.

This paper makes use of data from the AAVSO Photometric All Sky Survey, whose funding has been provided by the Robert Martin Ayers Sciences Fund. This research made use of Astropy, a community-developed core Python package for Astronomy (Astropy Collaboration et al. 2013), and Matplotlib library (Hunter 2007).

This project used public archival data from the Dark Energy Survey (DES). Funding for the DES Projects has been provided by the U.S. Department of Energy, the U.S. National Science Foundation, the Ministry of Science and Education of Spain, the Science and Technology Facilities Council of the United Kingdom, the Higher Education Funding Council for England, the National Center for Supercomputing Applications at the University of Illinois at Urbana-Champaign, the Kavli Institute of Cosmological Physics at the University of Chicago, the Center for Cosmology and Astro-Particle Physics at the Ohio State University, the Mitchell Institute for Fundamental Physics and Astronomy at Texas A&M University, Financiadora de Estudos e Projetos, Fundação Carlos Chagas Filho de Amparo à Pesquisa do Estado do Rio de Janeiro, Conselho Nacional de Desenvolvimento Científico e Tecnológico and the Ministério da Ciência, Tecnologia e Inovação, the Deutsche Forschungsgemeinschaft, and the Collaborating Institutions in the Dark Energy Survey. The Collaborating Institutions are Argonne National Laboratory, the University of California at Santa Cruz, the University of Cambridge, Centro de Investigaciones Energéticas, Medioambientales y Tecnológicas-Madrid, the University of Chicago, University College London, the DES-Brazil Consortium, the University of Edinburgh, the Eidgenössische Technische Hochschule (ETH) Zürich, Fermi National Accelerator Laboratory, the University of Illinois at Urbana-Champaign, the Institut de Ciències de l’Espai (IEEC/CSIC), the Institut de Física d’Altes Energies, Lawrence Berkeley National Laboratory, the Ludwig-Maximilians Universität München and the associated Excellence Cluster Universe, the University of Michigan, the National Optical Astronomy Observatory, the University of Nottingham, the Ohio State University, the University of Pennsylvania, the University of Portsmouth, SLAC National Accelerator Laboratory, Stanford University, the University of Sussex, and Texas A&M University.

## REFERENCES

- Astropy Collaboration, Robitaille, T. P., Tollerud, E. J., et al. 2013, *A&A*, 558, A33
- Bechtol, K., Drlica-Wagner, A., et al. 2015, arXiv:1503.02584
- Belokurov, V., Zucker, D. B., Evans, N. W., et al. 2006, *ApJ*, 647, L111
- Belokurov, V., Walker, M. G., Evans, N. W., et al. 2008, *ApJ*, 686, L83
- Belokurov, V., Irwin, M. J., Koposov, S. E., et al. 2014, *MNRAS*, 441, 2124
- Bertin, E., & Arnouts, S. 1996, *A&AS*, 117, 393
- Bertin, E. 2011, *Astronomical Data Analysis Software and Systems XX*, 442, 435
- Bressan, A., Marigo, P., Girardi, L., et al. 2012, *MNRAS*, 427, 127
- Brown, T. M., Tumlinson, J., Geha, M., et al. 2014, *ApJ*, 796, 91
- Desai, S., Armstrong, R., Mohr, J. J., et al. 2012, *ApJ*, 757, 83
- Frebel, A., Simon, J. D., Geha, M., & Willman, B. 2010, *ApJ*, 708, 560
- Grillmair, C. J. 2009, *ApJ*, 693, 1118
- Hunter, J. D. 2007, *Computing in Science and Engineering*, 9, 90
- Irwin, M. J., Belokurov, V., Evans, N. W., et al. 2007, *ApJ*, 656, L13
- Jerjen, H. 2010, *Advances in Astronomy*, 2010, 434390
- Kim, D., & Jerjen, H. 2015, *ApJ*, 799, 73
- Kim, D., Jerjen, H., Milone, A. P., Mackey, D., & Da Costa, G. S. 2015, *ApJ*, 803, 63
- Kim, D., Jerjen, H., Mackey, D., Da Costa, G. S., & Milone, A. P. 2015, arXiv:1503.08268
- Kirby, E. N., Simon, J. D., Geha, M., Guhathakurta, P., & Frebel, A. 2008, *ApJ*, 685, L43
- Kroupa, P. 2001, *MNRAS*, 322, 231
- Koposov, S., Belokurov, V., Evans, N. W., et al. 2008, *ApJ*, 686, 279
- Koposov, S. E., Belokurov, V., Torrealba, G., & Wyn Evans, N. 2015, arXiv:1503.02079
- Koposov, S. E., Casey, A. R., Belokurov, V., et al. 2015, arXiv:1504.07916
- Laevens, B. P. M., Martin, N. F., Sesar, B., et al. 2014, *ApJ*, 786, L3
- Laevens, B. P. M., Martin, N. F., Ibata, R. A., et al. 2015, arXiv:1503.05554
- Martin, N. F., Ibata, R. A., Chapman, S. C., Irwin, M., & Lewis, G. F. 2007, *MNRAS*, 380, 281
- Martin, N. F., de Jong, J. T. A., & Rix, H.-W. 2008, *ApJ*, 684, 1075
- Martin, N. F., Nidever, D. L., Besla, G., et al. 2015, *ApJ*, 804, L5
- Mohr, J. J., Armstrong, R., Bertin, E., et al. 2012, *Proc. SPIE*, 8451, 84510D
- Muñoz, R. R., Geha, M., & Willman, B. 2010, *AJ*, 140, 138
- Norris, J. E., Yong, D., Gilmore, G., & Wyse, R. F. G. 2010, *ApJ*, 711, 350
- Pawlowski, M. S., McGaugh, S. S., & Jerjen, H. 2015, arXiv:1505.07465
- Sand, D. J., Strader, J., Willman, B., et al. 2012, *ApJ*, 756, 79
- Shanks, T., Metcalfe, N., Chehade, B., et al. 2015, arXiv:1502.05432
- Schlafly, E. F., & Finkbeiner, D. P. 2011, *ApJ*, 737, 103
- Schlegel, D. J., Finkbeiner, D. P., & Davis, M. 1998, *ApJ*, 500, 525
- Simon, J. D., & Geha, M. 2007, *ApJ*, 670, 313
- Simon, J. D., Geha, M., Minor, Q. E., et al. 2011, *ApJ*, 733, 46
- Simon, J. D., Drlica-Wagner, A., Li, T. S., et al. 2015, arXiv:1504.02889
- Taylor, M. B. 2005, *Astronomical Data Analysis Software and Systems XIV*, 347, 29
- The Dark Energy Survey Collaboration 2005, arXiv:astro-ph/0510346
- Walker, M. G., Mateo, M., Olszewski, E. W., et al. 2015, arXiv:1504.03060
- Walsh, S. M., Jerjen, H., & Willman, B. 2007, *ApJ*, 662, L83
- Walsh, S. M., Willman, B., & Jerjen, H. 2009, *AJ*, 137, 450
- Weisz, D. R., Dolphin, A. E., Skillman, E. D., et al. 2014, *ApJ*, 789, 147
- Willman, B., Blanton, M. R., West, A. A., et al. 2005, *AJ*, 129, 2692
- Willman, B., & Strader, J. 2012, *AJ*, 144, 76
- York, D. G., Adelman, J., Anderson, J. E., Jr., et al. 2000, *AJ*, 120, 1579
- Zucker, D. B., Belokurov, V., Evans, N. W., et al. 2006, *ApJ*, 643, L103